Seasonal and Long-Term Coupling between Wintertime Storm Tracks and Sea Surface Temperature in the North Pacific

BOLAN GAN AND LIXIN WU

Physical Oceanography Laboratory, Ocean University of China, Qingdao, China

(Manuscript received 2 October 2012, in final form 16 February 2013)

ABSTRACT

In this study, a lagged maximum covariance analysis (MCA) of the wintertime storm-track and sea surface temperature (SST) anomalies derived from the reanalysis datasets shows significant seasonal and long-term relationships between storm tracks and SST variations in the North Pacific. At seasonal time scales, it is found that the midlatitude warm (cold) SST anomalies in the preceding fall, which are expected to change the tropospheric baroclinicity, can significantly reduce (enhance) the storm-track activities in early winter. The storm-track response pattern, however, is in sharp contrast to the forcing pattern, with warm (cold) SST anomalies in the western–central North Pacific corresponding to a poleward (equatorward) shift of storm tracks. At interannual-to-decadal time scales, it is found that the wintertime SST and storm-track anomalies are mutually reinforced up to 3 yr, which is characterized by PDO-like SST anomalies with warming in the western–central domain coupled with basin-scale positive storm-track anomalies extending along 50°N.

1. Introduction

Synoptic-scale baroclinic eddies prevalent in the midlatitudes aloft, referred to as storm tracks (Blackmon et al. 1977), influence not only local weather by affecting precipitation, cloudiness, and winds but also climate by transporting large amounts of heat, moisture, and momentum poleward and interacting with the planetary-scale flow (e.g., Trenberth and Hurrell 1994; Chang et al. 2002; Kug et al. 2010). Furthermore, it is found that storm tracks and the underlying ocean can interact with each other. The differential heat supply across a midlatitude frontal zone associated with strong sea surface temperature (SST) gradients is suggestive of maintaining the surface baroclinicity and thus sustains the development of storm tracks (Nakamura et al. 2004; Taguchi et al. 2009). At the same time, storm tracks can in turn influence the ocean by means of modulating the upper-level jet streams and transferring the mean westerly momentum downward to maintain the surface westerlies (e.g., Lau and Holopainen 1984; Nakamura et al. 2004; Sampe et al. 2010). Therefore, understanding of changes in the intensity, frequency, and geographical positions of storm tracks and potential association with SST variability will be help in understanding potential predictability of the extratropical climate variability.

Observational evidence has indicated that the North Pacific storm tracks exhibit remarkable seasonal to interdecadal variability. On seasonal time scales, storm tracks undergo not only significant migration in its latitudinal position but also striking midwinter suppression in its climatological intensity, despite the strong tropospheric baroclinicity (Nakamura 1992; Christoph et al. 1997; Zhang and Held 1999; Chang 2001). On interannual time scales, it is found that storm tracks are intimately linked with the El Niño–Southern Oscillation (ENSO) cycle, with equatorward and downstream shift during the El Niño events and opposite behavior during the La Niña events (e.g., Trenberth and Hurrell 1994; Zhang and Held 1999). On decadal time scales, the reanalysis data spanning the last half of the twentieth century indicate a significant transition from a weak to a strong storm-track regime during the early 1970s (e.g., Chang and Fu 2002; Nakamura et al. 2002; Lee et al. 2011). As for the mechanism of the seasonal and interannual variations of storm tracks, Chang (2001) found that diabatic heating and eddy structure play a critical role in the seasonal and interannual variations, respectively. Nakamura et al. (2004) also highlighted the trapping effect of subtropical

Corresponding author address: Dr. Lixin Wu, Physical Oceanography Laboratory, Ocean University of China, 5 Yushan Road, Qingdao 266003, China.
E-mail: lxwu@ouc.edu.cn

DOI: 10.1175/JCLI-D-12-00724.1

jet on the efficiency of eddies' capability to tap into the baroclinicity of mean flow in winter. For the decadal variations, previous studies propose a close link with the dominant modes of the extratropical climate variability, including the Arctic Oscillation (AO), Pacific decadal oscillation (PDO), and Pacific–North America (PNA) pattern (e.g., Chang and Fu 2002; Rivière and Orlanski 2007; Lee et al. 2011; Pinto et al. 2011). However, the physical mechanism involved still remains poorly understand.

Recently, observational and modeling studies generally indicate that storm tracks are important for the air–sea coupling in the midlatitudes. It has been found in observations that the North Pacific SST anomalies (SSTAs) can significantly influence the large-scale atmospheric mean circulation in early winter, with a signal resembling the PNA pattern (Frankignoul and Sennéchael 2007; Frankignoul et al. 2011; Taguchi et al. 2012). This atmospheric response is suggested to act as a key process to sustain decadal climate variability (e.g., Latif and Barnett 1994; Schneider et al. 2002; Wu et al. 2003; Kwon and Deser 2007). In generating the stationary response in barotropic structure, the anomalous storm-track activities responding to changes in the surface baroclinicity induced by the SSTAs are revealed as a critical factor (e.g., Peng and Whitaker 1999; Kushnir et al. 2002; Taguchi et al. 2012). Specifically, the transient eddy feedback underlying the anomalous storm tracks regulates the atmospheric response by interacting with the direct baroclinic response to the SST-induced heating anomalies, which suggests the potential importance of the association between the SSTAs and storm tracks in regulating the atmospheric responses.

Acting as an essential part in the North Pacific climate variation, storm-track variability is likely to be connected with the SSTAs on different time scales. However, the direct relationship between storm tracks and SST has not been clearly identified. In this study, the associations between the wintertime storm-track and SST variations over the North Pacific at seasonal and longer time scales are investigated based on the lagged maximum covariance analysis (Frankignoul and Sennéchael 2007). It is found that at seasonal time scales SSTAs in the preceding fall can significantly influence storm tracks in early winter, manifesting an intensification of storm tracks by the cold SSTAs in the North Pacific. This storm-track responding pattern, however, is in sharp contrast to the pattern when storm tracks lead SSTAs, characterized by a meridional shift of storm tracks. On interannual and longer time scales, the wintertime SST and storm-track anomalies are mutually reinforced, with the corresponding covariance patterns resembling the dominant modes of North Pacific SST and storm-track decadal variability in winter, respectively.

The paper is arranged as follows: Section 2 presents the datasets and method we used. The seasonal association between storm tracks and SST in the cold season is described in section 3, followed by the wintertime association at long-term time scales in section 4. Summary and discussion are given in section 5.

2. Data and method

Atmospheric variables including the meridional wind velocity, surface wind stress and net surface heat flux (the sum of shortwave, longwave, latent, and sensible heat fluxes) are obtained from the ensemble-mean fields of the Twentieth-Century Reanalysis dataset version 2 (20CRv2) with a horizontal resolution of $2° \times 2°$ (Compo et al. 2011). SST is taken from the Met Office Hadley Centre Sea Ice and Sea Surface Temperature version 1 (HadISST1) dataset with 1° spatial resolution (Rayner et al. 2003), and other oceanic variables including subsurface temperature, three-dimensional velocity, and sea surface height are taken from the Simple Ocean Data Assimilation (SODA; version 2.2.4; Carton and Giese 2008). The newly available 20CRv2 assimilates only synoptic surface pressure observations and prescribes observed monthly SST and sea ice distributions as boundary conditions for the atmosphere. Intercomparison over the second half century of the 20CRv2 with other reanalyses indicates that it is generally of high quality and reliable to assess changes in the North Pacific winter storm tracks (e.g., Compo et al. 2011; Donat et al. 2011). Here the temporal coverage of all variables used in this study is from 1910 to 2008 to avoid possible data scarcity prior to 1910.

In this study, storm tracks are defined as the bandpass-filtered (2–8 days) 300-mb meridional wind velocity variance (Blackmon et al. 1977; Chang and Fu 2002; Sampe et al. 2010). The storm-track activity represented by the 850-mb poleward eddy flux of sensible heat has also been examined and similar results were obtained in general. Monthly anomalies of all field quantities are obtained by subtracting the climatological monthly means and removing the linear trend based on a least squares regression. Given the far-reaching impact of ENSO on the North Pacific climate (Alexander et al. 2002), much of the ENSO influence is removed by subtracting the relevant part from the monthly anomalies of each field, based on a linear regression onto the first two principal components of the SSTAs in the tropical Pacific between 20°S and 20°N. Taking into account the strong seasonality of ENSO and lagged response of extratropical ocean to ENSO, the seasonally varying regression coefficients are used for the removal of ENSO influence. Specifically, a total of 12 regression

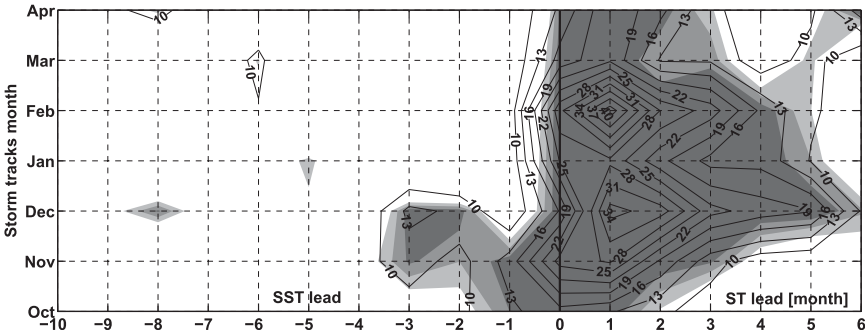

FIG. 1. SC of the first MCA mode between storm tracks and SSTAs in the North Pacific (20°–60°N, 120°E–120°W) during the cold season. Shaded area exceeds 85% (light), 90% (heavy), and 95% (heaviest) confidence level based on the Monte Carlo test. Ordinate is the storm-track calendar month and abscissa is the lag in month: positive (negative) for storm tracks (SST) leading SST (storm tracks).

coefficients are derived from a 2-month lagged regression for oceanic variables and simultaneous regression for atmospheric variables at each grid point and in each calendar month. To reduce the sampling error, these regression coefficients are then smoothed through a 3-month running mean. Much of the ENSO influence is effectively removed based on this linear method (as seen in Figs. 2, 9).

The lagged maximum covariance analysis (MCA) has been widely used to study the influence of the ocean on the atmosphere in the midlatitudes (e.g., Czaja and Frankignoul 2002; Frankignoul and Sennéchael 2007; Gastineau and Frankignoul 2012). Here, the MCA is performed to investigate the relationship between storm tracks and SST in the North Pacific. To identify whether the MCA modes are meaningful, statistical significance is estimated using the Monte Carlo test, a nonparametric approach, in which MCA is repeated 100 times using the original SSTAs with storm-track time series randomly scrambled to reduce the influence of serial autocorrelation. The probability distribution function of the obtained 100 values of squared covariance (SC), squared covariance fraction (SCF), and correlation coefficient is then constructed to rank the significance of the corresponding statistics.

In this study, the homogeneous map for SST and heterogeneous map for storm tracks, derived from the regression patterns against the SST time series of the first MCA mode when SST leads storm tracks, are shown to investigate the influence of the SSTAs on the storm-track activities. When studying the oceanic response to the storm-track variations, the heterogeneous map for SST and homogeneous map for storm tracks, which are projections on the storm-track time series of the first MCA mode when storm tracks lead SST, are shown.

3. Seasonal association between storm tracks and SST

We first examine the seasonal association between SST and storm tracks during the cold season, by applying the MCA as a function of time lag in month to the monthly SST and storm-track anomalies over the North Pacific (20°–60°N, 120°E–120°W). The SC of the first MCA mode exhibits a strong seasonal dependence and an asymmetry of the lead–lag, as shown in Fig. 1. Throughout the cold season, the SC is strong when storm tracks lead SST (positive lags), with two peaks in December and February at lag +1 month, indicating a predominant forcing by storm tracks. In contrast, the SC is much lower when SST leads storm tracks (negative lags). However, there are significant covariances when SST leads storm tracks in November and December by 2 and 3 months, indicating a potential influence of SSTAs in fall on storm tracks in early winter. Taking into account that the SCs are most significant in December, we mainly focused on December to explore the influence of SST on storm tracks.

a. Influence of SST on storm tracks

The maximum covariance patterns of the storm-track and SST anomalies are illustrated in Fig. 2, for the first corresponding MCA modes with storm tracks fixed in December and SST in September, October, December, and January, respectively. Note that to examine whether there is a potential influence from tropics, we extend the regression domain to 20°S. When SST leads storm tracks, it is found that SSTAs in the preceding fall can significantly influence storm tracks in early winter, such that the cold (warm) anomalies in the midlatitudes can enhance (reduce) the storm-track activities. The SST effecting on storm tracks in December occurs most

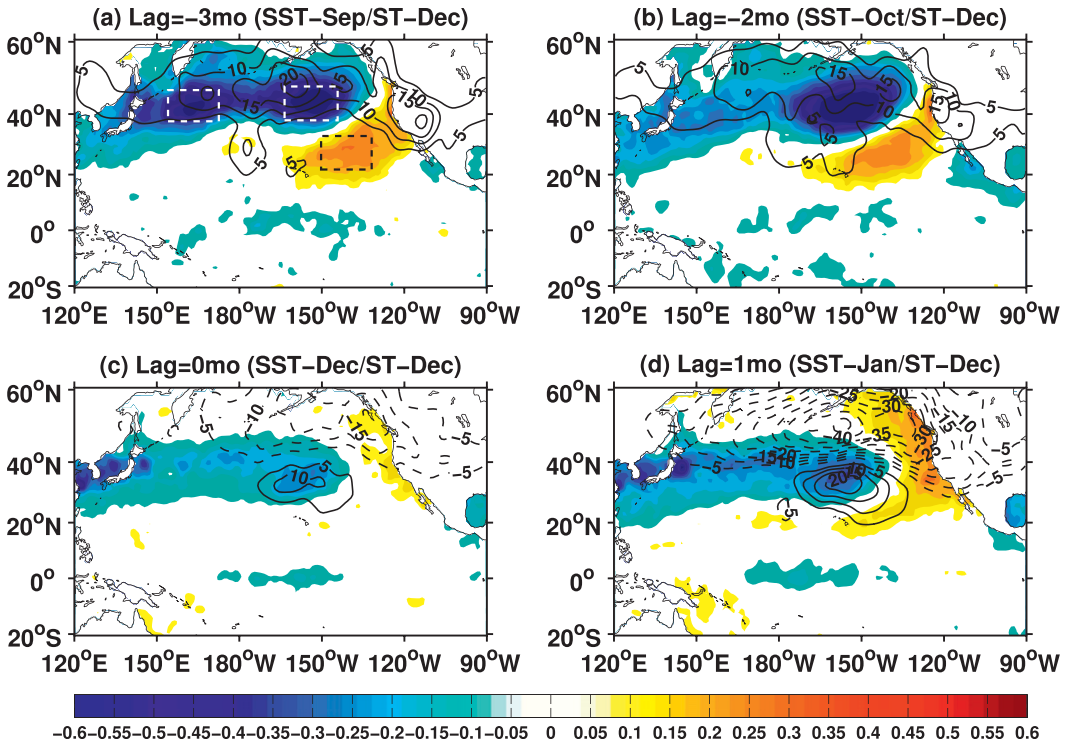

FIG. 2. Homogeneous maps for SST and heterogeneous maps for storm tracks corresponding to the first MCA modes with storm tracks fixed in December and SST lagging by (a) −3 and (b) −2 months. (c) Simultaneously heterogeneous maps for SST and storm tracks in December. (d) As in (a), but for the heterogeneous maps for SST and homogeneous maps for storm tracks in lag +1 month. Colors for SST are in degrees Celsius, and contours for storm tracks with negative values are dashed, contour intervals are 5 $m^2 s^{-2}$. The MCA time series have been normalized so that the typical amplitudes are given.

significantly in September, with the SCF of 59%, and exhibits a significant interannual variability superimposed on some low-frequency variability, as seen in the time coefficients of the SST leading mode (Fig. 3a). The corresponding SST mode shows cold anomalies dominant in the north of 30°N with an amplitude of −0.6°C occurring along 45°N, accompanied by warm anomalies in the southeastern region of North Pacific (Fig. 2a).

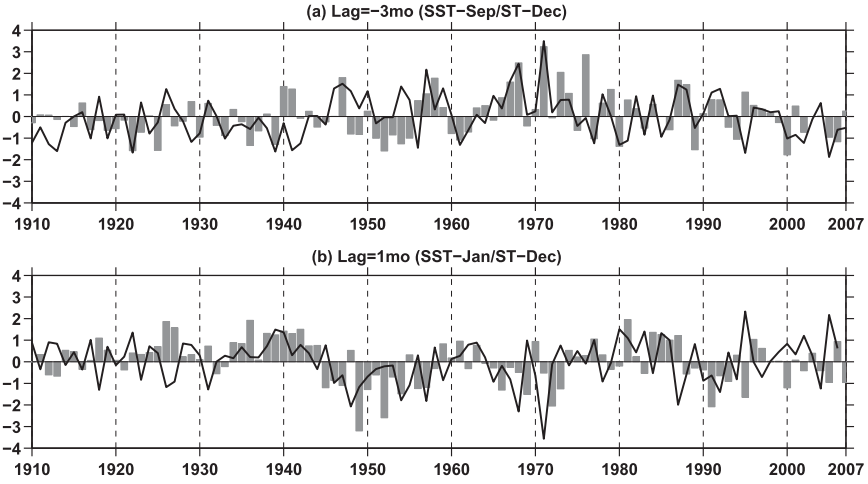

FIG. 3. Normalized time series of storm tracks (line) in December and SST (bar) lagging by (a) −3 and (b) +1 months derived from the corresponding first MCA modes.

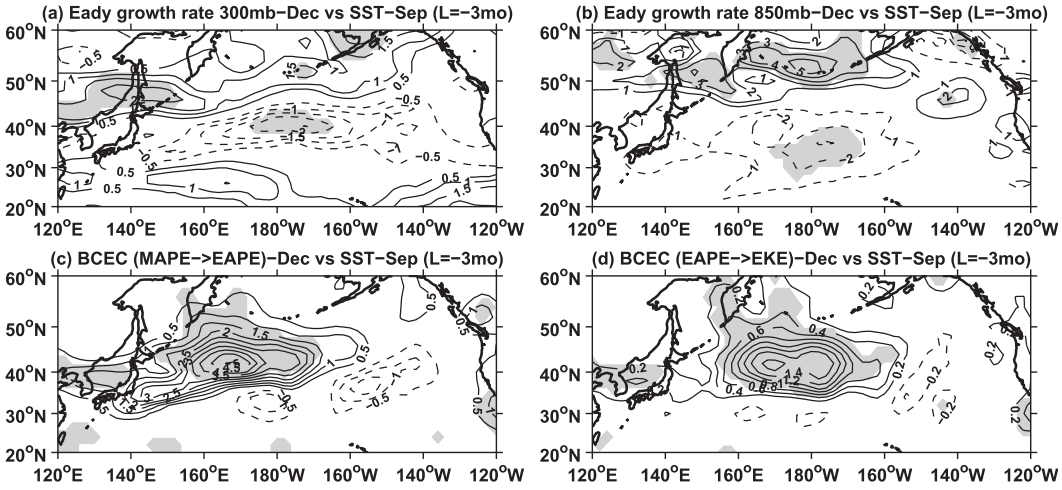

FIG. 4. Regression of the maximum Eady growth rate (10^{-2} day^{-1}) at (a) 300 and (b) 850 mb; baroclinic energy conversion from (c) MAPE to EAPE and (d) EAPE to EKE (W m^{-2}) at 300 mb in December onto the lag −3 SST time series (bar in Fig. 3a) in September. Dashed contours denote negative values and shaded areas exceed 95% confidence level.

Compared to the North Pacific SSTAs, the tropical SSTAs are much smaller, suggesting that the remote influence from tropics is negligible. In association with the prior SSTAs in September, there are positive storm-track anomalies in December extending along 50°N to the north of the position of its climatological peak, with the maximum amplitude of 20 m^2 s^{-2}, implying a sensitivity of about 33 m^2 s^{-2} °C^{-1}. The storm-track time series in Fig. 3a is well correlated with the SST time series, with the correlation coefficient of 0.49, indicating that the SST variability in September may explain about 24% of the variance of storm-track variability in December. Furthermore, to determine which center of the SSTA pattern has the strongest influence on storm tracks, we project the storm-track anomalies onto three SST time series that are derived from the area-averaged SSTAs in the boxes centered on the main centers of action (see Fig. 2a). It is found that the storm-track anomaly pattern (not shown) mainly associated with the eastern cold center and, to a lesser extent, the southeastern warm center resembles the corresponding MCA pattern, with the maximum response of 25 m^2 s^{-2} °C^{-1}. This is likely to suggest a dominant role of the eastern North Pacific SSTAs in September in affecting storm tracks after 3 months. Note that, given its independence from the MCA, this calculation also suggests that the MCA results are robust. Compared to the maximum covariance pattern at lag −3, the pattern at lag −2 appears to change little, except that the western cold SSTAs are weakened significantly and the eastern cold SSTAs are intensified (Fig. 2b).

To understand the storm-track response to SST, the maximum Eady growth rate, defined as $\sigma = 0.31gN^{-1}T^{-1}|\partial T/\partial y|$ in which T is the temperature, g is the gravitational acceleration, and N is the Brunt–Väisälä frequency (Lindzen and Farrell 1980), is calculated to measure the linear baroclinic instability of atmosphere that provides a baroclinic source for the development of storm tracks. In addition, given that a number of factors can influence the efficiency of eddies' ability to tap into the baroclinicity of time-mean flow (e.g., Chang 2001), it is necessary to diagnose the local baroclinic energy conversion (BCEC). The BCEC from mean available potential energy (MAPE) to eddy available potential energy (EAPE) and from EAPE to eddy kinetic energy (EKE) are defined as follows:

$$\mathrm{BCEC(MAPE \rightarrow EAPE)} = -C_1\left(\frac{p_0}{p}\right)^{R/C_p}\left(-\frac{d\Theta}{dp}\right)^{-1}\left(\overline{u'T'}\frac{\partial\overline{T}}{\partial x}+\overline{v'T'}\frac{\partial\overline{T}}{\partial y}\right),$$

$$\mathrm{BCEC(EAPE \rightarrow EKE)} = -C_1(\overline{\omega'T'}),$$

where $C_1 = (p_0/p)^{(C_v/C_p)}(R/g)$ and R, ω, Θ, and C_p (C_v) are the gas constant for dry air, vertical pressure (p) velocity, potential temperature, and specific heat capacity of dry air at the constant pressure (volume), respectively. More details are described in Cai et al. (2007). These three quantities have been utilized in a range of studies on the storm-track variability as well as changes under global warming (e.g., Yin 2005; Mizuta et al. 2011; Wu et al. 2011).

Figure 4 illustrates the regression maps of the maximum Eady growth rate and baroclinic energy conversion against the SST leading time series in September

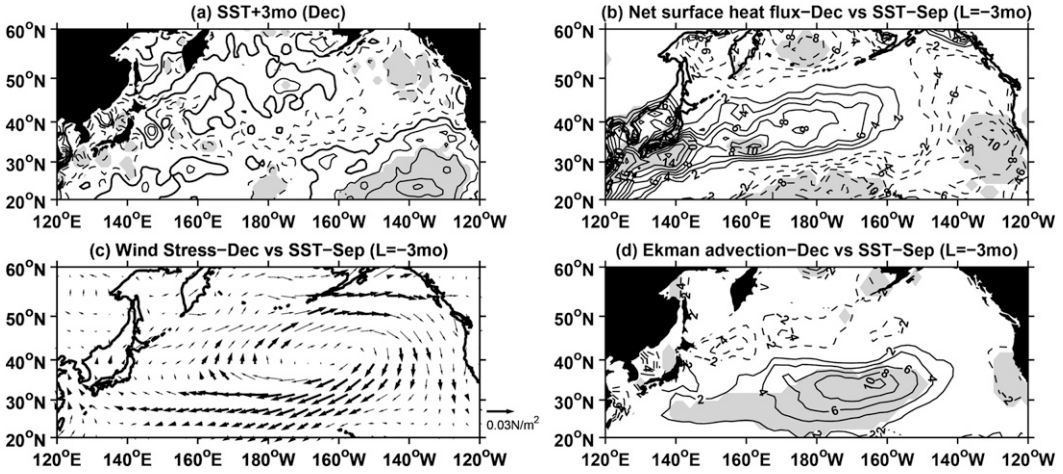

FIG. 5. Regression of the (a) SST, (b) net surface heat flux, (c) surface wind stress ($N\,m^{-2}$), and (d) Ekman advection in December onto the lag −3 SST time series (bar in Fig. 3a) in September. Contour interval is 0.04°C for (a) and $2\,W\,m^{-2}$ for (b),(d). Dashed contours denote negative values. Shaded areas and thick arrows exceed the 95% confidence level. Note that negative regression coefficients for the net surface heat flux signify the heat transferred from the ocean into the atmosphere and vice versa.

shown in Fig. 3a. The results suggest that the poleward strengthening of the tropospheric baroclinicity associated with the midlatitude cold SSTAs in the preceding fall is presumed to be responsible for the poleward intensification of storm tracks in early winter. As seen in Fig. 4a, the Eady growth rate at 300 mb increases in the northern part of the climatological baroclinicity domain with the maximum located over the Sakhalin Island and decreases over the central North Pacific along 40°N, indicating a northward shift and intensification of the upper-tropospheric baroclinicity. Such changes in the baroclinic instability are more evident in the lower troposphere. As seen in the Fig. 4b, the Eady growth rate at 850 mb increases to the north of 45°N significantly, with the maximum located in the upstream of the center of the corresponding storm-track anomalies (see Fig. 2a), and deceases to the south. These tropospheric baroclinicity changes are clearly associated with the downstream increase of the eddy activities, since more available potential energy is likely to be tapped into the baroclinic eddies, which is further confirmed by the diagnosis of BCEC. The energy conversions from MAPE to EAPE and from EAPE to EKE are significantly increased over the western and central North Pacific, indicative of the enhanced downstream development of storm tracks (Figs. 4c,d). A further inspection finds that the changes in the baroclinic instability are primarily determined by the meridional temperature gradient changes. In addition, a recent study by Nakamura and Yamane (2010) suggests that the SSTAs in fall may well be generated during summer.

Finally, to investigate the feedback of the storm-track response in early winter onto the ocean, the net surface heat flux and surface wind stress in December are regressed on the SST leading time series in September. It is found that both forcings (the net surface heat flux and surface wind stress) on the ocean mostly act as negative feedbacks on the SSTAs. The regression of the net surface heat flux shows that anomalous heat in the south of Japan and the central North Pacific is transferred from atmosphere into ocean, and the opposite action significantly occurred in the southeastern part of North Pacific (Fig. 5b). As seen by comparison with the December SSTA pattern in Fig. 5a, these anomalous heat fluxes generally act to damp the SSTAs therein. In addition, the regression of the surface wind stress shows a basin-scale anticyclonic anomaly in the North Pacific, especially a significant large westward wind stress anomaly in the southern part of the domain (Fig. 5c). The associated poleward Ekman warm advection acts to damp the cold SSTAs in the southern–central North Pacific, as seen in Fig. 5d.

b. Storm-track forcing on SST

When storm tracks lead SST, it is found that a meridional shift of storm tracks tend to force a horseshoe pattern of SSTAs confined in the North Pacific (Fig. 2d). As seen in Fig. 1, the forcing of storm tracks in December leads to the strongest SST responses in January, with the SCF of 64%. The associated storm-track pattern shown in Fig. 2d has a meridional dipole structure whose node coincides with the position of its climatological peak, indicating a meridional shift of storm tracks.

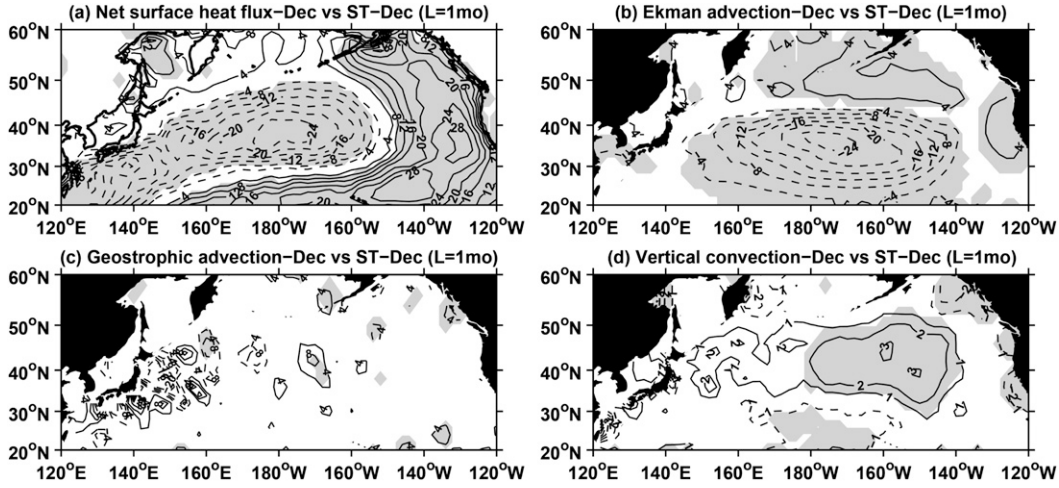

FIG. 6. Simultaneous regression of the (a) net surface heat flux, (b) Ekman advection, (c) geostrophic advection, and (d) vertical convection onto the lag +1 storm-track time series (line in Fig. 3b) in December. Dashed contours denote negative values and shaded areas exceed 95% confidence level. Note that negative regression coefficients for the net surface heat flux signify the heat transferred from the ocean into the atmosphere and vice versa. Units are $\mathrm{W\,m^{-2}}$.

This is in sharp contrast with the storm-track pattern responding to the North Pacific SSTAs in fall (see Figs. 2a,b). This pattern also resembles a dominant storm-track mode in December, implied from the first empirical orthogonal function (EOF) of the storm-track anomalies (not shown). The time coefficients of the storm-track leading mode exhibits significant interannual and decadal variability (Fig. 3b). The ocean response to the southward shift of storm tracks in January has cold SSTAs along 40°N in the western and central North Pacific, with the maximum of −0.5°C off the east coast of Japan, and warm SSTAs along the western coast of North America (Fig. 2d). The corresponding SST time series in Fig. 3b is well correlated with the prior storm-track time series (correlation coefficient is 0.56) and shows a substantial decadal variability. The simultaneous MCA modes of storm tracks and SST in December bear great similarities with the MCA patterns obtained at lag 1 but have lower magnitudes compared to the latter (Fig. 2c).

To further investigate the processes responsible for the SSTAs induced by storm tracks in early winter, we examine the mixed layer heat budget following Kwon and Deser (2007),

$$\rho C_p h \frac{\partial T}{\partial t} = Q_{\mathrm{net}} - (\rho C_p h \mathbf{V}_{\mathrm{Ek}} \cdot \nabla T) - (\rho C_p h \mathbf{V}_{\mathrm{geo}} \cdot \nabla T) - \left(\rho C_p h w \frac{\partial T}{\partial z}\right) + \mathrm{residual},$$

where ρC_p is the volumetric heat capacity of seawater; T is the SST; Q_{net} is the net surface heat flux; h is the mixed layer depth; $\mathbf{V}_{\mathrm{Ek}}$ is the Ekman velocity; $\mathbf{V}_{\mathrm{geo}}$ is the geostrophic velocity; w is the vertical velocity; and ''residual'' denotes all terms not listed including diffusion. Note that we define positive Q_{net} to be downward (i.e., heat is transferred from atmosphere into ocean).

The four leading terms on the right hand side of the above equation (i.e., the net surface heat flux, the Ekman advection, the geostrophic advection, and the vertical convection) are simultaneously regressed on the lag 1 storm-track time series in December. It is found that both the surface heat flux and Ekman advection contribute to the generation of the SST mode. Specifically, as seen in the comparison of Fig. 2d with Fig. 6, the warm SSTAs along the western coast of North America is primarily determined by the surface heat flux forcing, whereas in the central North Pacific the cold SSTAs are attributed to both the heat flux and Ekman cold advection associated with a significant basin-scale cyclonic wind stress anomaly centered at 43°N, 160°W (not shown). Further decomposition of the total Ekman advection ($\mathbf{V}_{\mathrm{Ek}} \cdot \nabla \mathrm{SST}$) into $\mathbf{V}'_{\mathrm{Ek}} \cdot \nabla \overline{\mathrm{SST}}$, $\overline{\mathbf{V}_{\mathrm{Ek}}} \cdot \nabla \mathrm{SST}'$, and $\mathbf{V}'_{\mathrm{Ek}} \cdot \nabla \mathrm{SST}'$, where the overbar denotes the December–February (DJF) mean and the prime denotes the deviations from the DJF mean, finds that the advection of the mean SST by the anomalous Ekman current dominates over other components. This indicates a direct forcing of the cold SSTAs by the storm-track-induced Ekman advection. The geostrophic advection (Fig. 6c) associated with the storm-track anomalies has comparable but insignificant magnitude in the Kuroshio region, which implies a strong contribution from the ocean currents to the SSTAs therein as suggested by recent

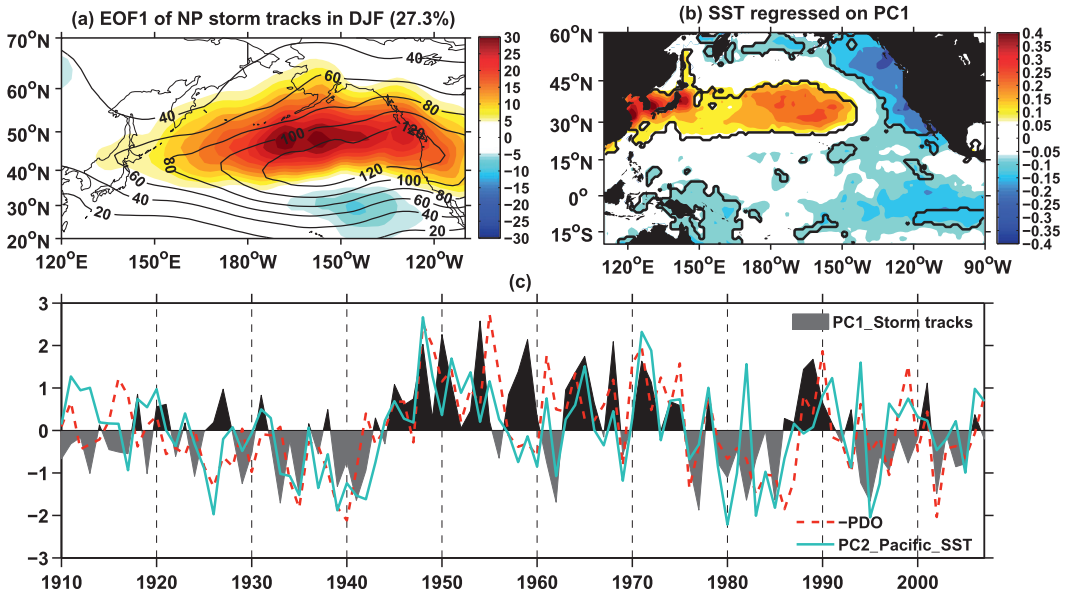

FIG. 7. (a) Leading EOF mode of the seasonal-mean storm-track anomalies (colors) superimposed by its climatology (contours) in DJF over the North Pacific (20°–70°N, 120°E–110°W). (b) Corresponding regression of SST onto the normalized leading PC1 of storm tracks shown in (c). The thick contours indicate the 95% confidence level. (c) Normalized PC1 of storm tracks in shading, together with the PDO index (red dashed line) and the PC2 of DJF-mean SSTAs in the Pacific (20°S–60°N, 120°E–100°W).

studies (e.g., Qiu 2000; Kelly and Dong 2004; Kwon and Deser 2007). Compared with the other three terms, the vertical convection with much lower magnitude (Fig. 6d) generally act to damp the cold SSTAs in the western–North Pacific.

4. Long-term association between storm tracks and SST

a. Decadal variability of storm tracks

Taking advantage of the long temporal coverage of the 20CRv2, we first investigate the decadal variability of storm tracks based on the EOF analysis. It is applied to the winter-averaged storm-track anomalies in DJF over the North Pacific (20°–70°N, 120°E–110°W), without removal of the ENSO influence. The leading EOF of the wintertime storm-track variations accounts for 27% of the total variance. As seen in Fig. 7a, the spatial pattern of this mode, corresponding to one standard deviation of its principal component (PC1), has a peak over the eastern North Pacific that occurs slightly to the north of the climatological peak of the Pacific storm tracks. Given that the PC1 time series in Fig. 7c exhibits a distinct decadal variability, this mode clearly represents the decadal variations in the intensity of the wintertime storm tracks.

To explore the potential relationship between the SST and storm-track variations, the DJF-mean SSTAs in the Pacific are regressed onto the PC1 of storm tracks. It is found that the decadal variability of storm tracks is strongly associated with the North Pacific decadal mode linearly independent of ENSO. As seen in Fig. 7b, the regression of the winter SSTAs shows a PDO-like pattern, with significant warm SSTAs confined in the western and central North Pacific and cold ones surrounding it. Although there are some significant cold SSTAs in the tropics, the magnitude is somewhat smaller than the North Pacific ones. Indeed, the PC1 of storm tracks is negatively correlated with the DJF-mean PDO index defined as the PC1 of the monthly North Pacific SSTAs poleward of 20°N in Fig. 7c (correlation coefficient is −0.40; Mantua et al. 1997). To further examine the robustness of the relationship between SST and storm tracks, a singular value decomposition (SVD) is performed on the cross-covariance matrix between DJF-mean SST and storm-track anomalies in the Pacific, with ENSO influence removed based on the seasonally varying regression against the PC1 and PC2 of the tropical Pacific SSTAs. The leading SVD pair (not shown but see Fig. 9d), accounting for 55% of the SCF, has heterogeneous covariance structures largely similar to the leading EOF of storm tracks and the associated SST pattern. The correlation coefficients between the SVD time series of storm tracks and the corresponding PC1 is 0.91, confirming that the regression pattern in Fig. 7 captures the coupled pattern between storm tracks and

SST during boreal winter. Moreover, to test whether the regression pattern of SST is linearly independent of ENSO, we performed the EOF analysis on the DJF-mean SSTAs in the Pacific (20°S–60°N) including the tropical region. The second EOF of the Pacific winter SSTAs is found to be similar to the SST mode shown in Fig. 7b, which has been suggested to be a North Pacific mode linearly independent of ENSO (Deser and Blackmon 1995; Zhang et al. 1996). The corresponding PC2 time series is also well correlated with the PC1 of storm tracks with the correlation attaining 0.46 (Fig. 7c). Overall, the decadal variability of the wintertime storm tracks is closely related to the North Pacific decadal mode, which is linearly independent of ENSO.

b. Long-term connection

To further investigate the association between storm tracks and SST in winter at long time scales, we applied the MCA as a function of time lag in year to the DJF-mean SST and storm-track anomalies, with ENSO influence removed, in the North Pacific (20°–60°N, 120°E–120°W). As seen in Fig. 8, the SC of the first MCA mode shows a nearly symmetric structure with significant ones detected from lag −3 to 4 yr, indicating that storm tracks are coupled with SST during winter at interannual and longer time scales. In addition, the SCF is significant from lag −3 to 4 yr as well, with two peaks reaching 77% at both lag −2 (SST leading) and lag 3 (storm-track leading).

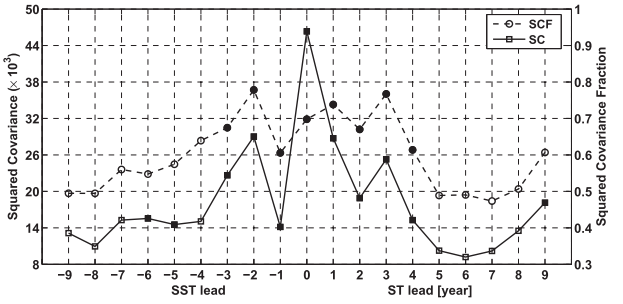

FIG. 8. SC (solid line) and SCF (dashed line) of the first MCA mode between seasonal-mean storm-track and SST anomalies in DJF over the North Pacific (20°–60°N, 120°E–120°W). Solid symbols indicate values significant at 95% confidence level based on the Monte Carlo test. Abscissa is the lag in year: positive (negative) for storm tracks (SST) leading SST (storm tracks).

Figure 9 illustrates the maximum covariance patterns of the storm-track and SST anomalies, for the first corresponding MCA modes at lag −3, −2, −1, 0, 1, and 3 yr. Again we extend the regression domain to 20°S to examine whether there is a potential influence from tropics. When SST leads storm tracks, a PDO-like pattern of North Pacific SSTAs tend to induce a basin-scale storm-track anomaly extending along 50°N to the north of the corresponding climatological peak. For example, as seen at lag −2 (Fig. 9b), the SST leading mode has warm anomalies confined in the western and central North Pacific, with the maximum SSTAs of ~0.7°C

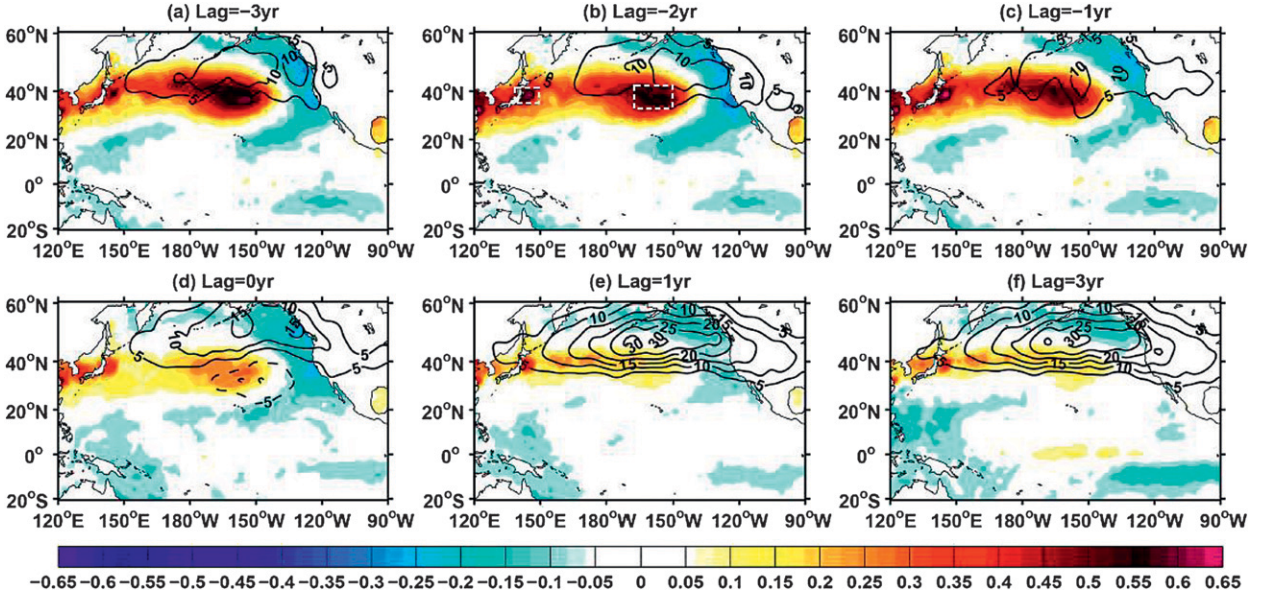

FIG. 9. Homogeneous maps for SST and heterogeneous maps for storm tracks in DJF corresponding to the first MCA modes with SST lagging by (a) −3, (b) −2, and (c) −1 yr. (d) Simultaneously heterogeneous maps for SST and storm tracks in DJF. (e),(f) As in (a),(c), but for the heterogeneous maps for SST and homogeneous maps for storm tracks in lag (e) +1 and (f) +3 yr. Colors for SST are in degrees Celsius, and contours for storm tracks with negative values are dashed (interval: 5 $m^2 s^{-2}$). The MCA time series have been normalized so that the typical amplitudes are given.

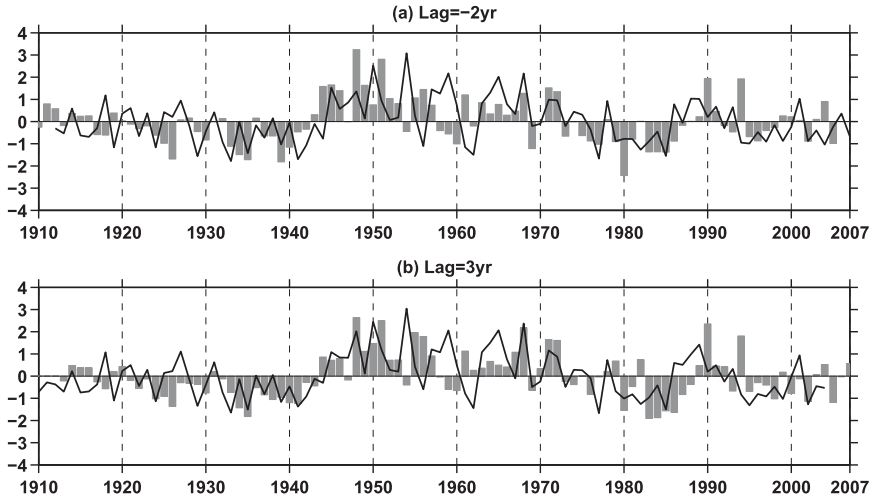

FIG. 10. Normalized time series of storm tracks (line) and SST (bar) at lag (a) −2 and (b) +3 yr derived from the corresponding first MCA modes.

occurring near the east coast of Japan at 40°N and hence in the Kuroshio–Oyashio Extension (KOE) region, and cold anomalies along the western coast of North America. This SST pattern is similar to the leading EOF of DJF-mean SSTAs in the North Pacific, which explains 30% of the total variance (excluding the ENSO impact). The corresponding SST time series in Fig. 10a exhibits a pronounced decadal variability, which has high correlation with the DJF-mean PDO index (−0.71). In responding to this SST mode after 2 yr, storm tracks have basin-scale positive anomalies to the north of 40°N, with a peak of 15 $m^2 s^{-2}$ located over the northeast of the warm SSTAs in the center of the domain (Fig. 9b), implying a sensitivity of 21 $m^2 s^{-2} °C^{-1}$. The corresponding storm-track time series displays a substantial decadal variability as well, that is significantly correlated with the prior SST time series (correlation coefficient is 0.45; Fig. 10a). By the lagged regression of the maximum Eady growth rate at 850 and 300 mb onto the lag −2 SST time series (Figs. 11a,b), it is found that the lower-tropospheric baroclinicity significantly strengthens to the north of 40°N, which are more consistent with the identified intensification of storm tracks as compared with the changes in the upper-tropospheric baroclinicity. This may indicate the important role played by the low-level baroclinicity in affecting storm tracks,

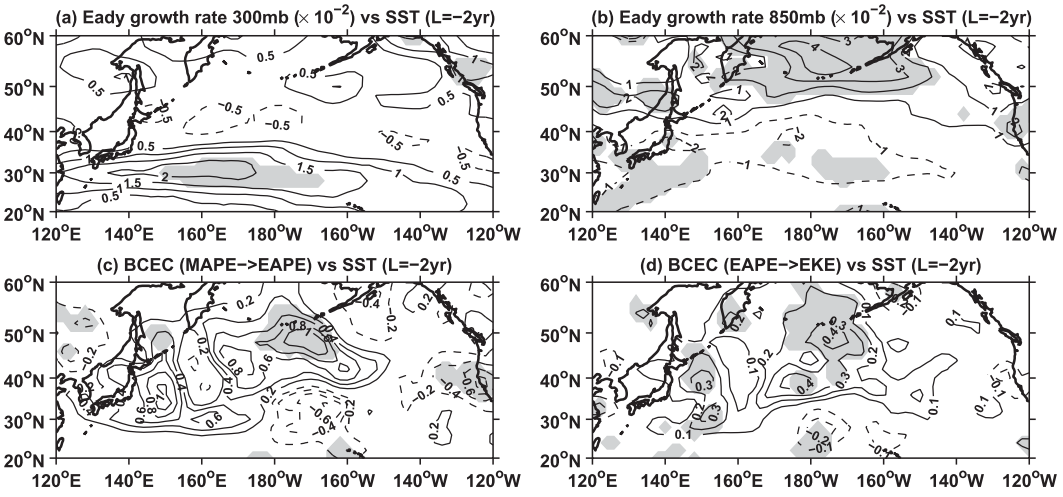

FIG. 11. Regression of the maximum Eady growth rate (10^{-2} day^{-1}) at (a) 300 and (b) 850 mb; baroclinic energy conversion from (c) MAPE to EAPE and (d) EAPE to EKE ($W m^{-2}$) at 300 mb in 2 yr later onto the lag −2 SST time series (bar in Fig. 10a). Dashed contours denote negative values and shaded areas exceed the 95% confidence level.

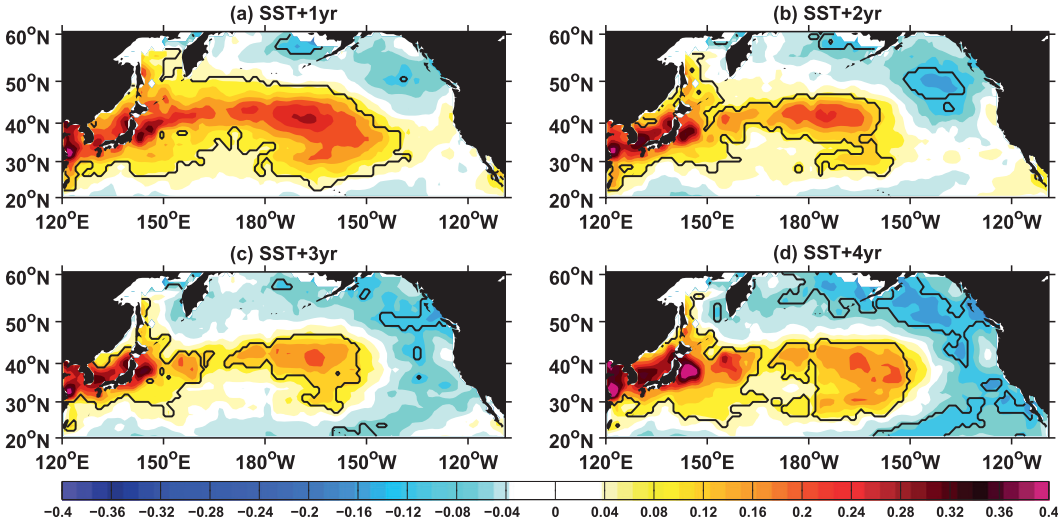

FIG. 12. Regression of SST in (a) 1, (b) 2, (c) 3, and (d) 4 yr later onto the preceding SST time series at lag −4. The thick contours indicate the 95% confidence level.

as suggested by recent studies (e.g., Nakamura et al. 2004; Sampe et al. 2010). In addition, the lagged regression of the local baroclinic energy conversion also shows significant positive anomalies in the central North Pacific (Figs. 11c,d), indicating that the baroclinic eddies are intensified through effectively tapping into more available potential energy. Note that the North Pacific SSTAs in Figs. 9a–c are larger than the tropical ones, suggesting a dominant influence of the local SST on storm tracks.

To investigate which positive center of the SST leading pattern at lag −2 may determine the storm-track responding pattern, we project the storm-track anomalies on two SST time series that are derived from the area-averaged SSTAs in the boxes centered on its main centers (Fig. 9b): 36.5°–41.5°N, 139.5°–147.5°E and 33.5°–42.5°N, 170.5°–148.5°W. It is found that the storm-track anomaly pattern associated with the western box resembles the corresponding MCA pattern, with the maximum response of 18 $m^2 s^{-2} °C^{-1}$, suggesting that the SSTAs in the KOE region play a dominant role in generating the storm-track anomalies at least 2 yr later. This also confirms the robustness of the MCA results.

Moreover, as seen from lag −3 to −1 (Figs. 9a–c), the warm SSTAs have a tendency to increase in the KOE west of 150°E but decrease in the central North Pacific, whereas the cold SSTAs seem to increase along the western coast of North America. To further examine this SST variation, a serial map of the SSTA field lagging by 1–4 yr is regressed onto the prior SST time series at lag −4, which may lead to possible predictability at longer time. The results shown in Fig. 12 indicate that the SSTAs in the western North Pacific have a stronger persistency than those in the central North Pacific. In addition, the cold SSTAs gradually emerge along the western coast of North America. This is probably attributable to a feedback of the storm-track response to the earlier SSTAs, which can be verified from the storm-track leading situation as follows.

As seen in Figs. 9e,f, in responding to the basin-scale positive storm-track anomalies, which resemble the leading EOF of storm tracks as shown in Fig. 7a, the SSTA pattern shows significant warm anomalies along 40°N, particularly in the KOE region, and cold anomalies north of 45°N. In addition, the time coefficients of storm-track and SST mode at lag 3 are well correlated with each other (correlation coefficient is 0.48; Fig. 10b), and both display a distinct decadal variability. Comparing Fig. 9a with Fig. 9f, it is worth noting that the storm-track leading pattern bears great similarities with the pattern responding to the decadal variations of North Pacific SSTAs, indicating that at interannual and longer time scales the North Pacific storm tracks and SST are mutually reinforced during boreal winter. A further inspection of the lagged regression of the mixed layer heat budget onto the lag −3 storm-track time series suggests that the cold SSTAs, especially in the Gulf of Alaska, are mainly attributed to the upward heat flux associated with the positive storm-track anomalies (see Fig. 13a). In addition, the anomalous Ekman warm advection along 40°N in association with a basin-scale anticyclonic wind stress anomaly centered at 50°N, 170°W is primarily responsible for the persistence of the warm SSTAs in the western and central North Pacific, except in the KOE west of 150°E (see Figs. 13b,c).

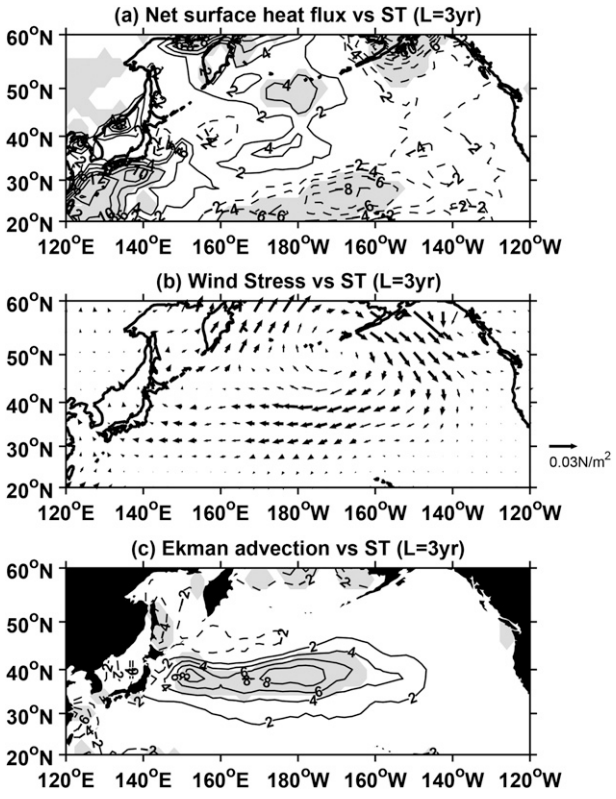

FIG. 13. Regression of the (a) net surface heat flux, (b) surface wind stress ($N\,m^{-2}$), and (c) Ekman advection in 3 yr later onto the lag +3 SST time series (line in Fig. 10b). Contour interval is $2\,W\,m^{-2}$ for (a),(c). Dashed contours denote negative values. Shaded areas and thick arrows exceed 95% confidence level. Note that negative regression coefficients for the net surface heat flux signify the heat transferred from the ocean into the atmosphere and vice versa.

5. Summary and discussion

The relationships between the wintertime storm-track and SST variations over the North Pacific at seasonal and long-term time scales are investigated based on the lagged MCA. The MCA results suggest that the wintertime storm-track anomalies in basin scale are significantly associated with the SSTAs in the North Pacific, but with different behaviors on seasonal and long-term time scales.

On seasonal time scales, it is found that SSTAs in the preceding fall can significantly influence storm tracks in early winter, such that the anomalously cold (warm) SST can induce significant positive (negative) storm-track anomalies in the north of 30°N, with the maximum response magnitude of $33\,m^2\,s^{-2}\,°C^{-1}$. Moreover, analyses of the maximum Eady growth rate and baroclinic energy conversion suggest that the poleward strengthening of the tropospheric baroclinicity associated with the midlatitude cold SSTAs in fall is presumed to be responsible for the poleward intensification of storm tracks in early winter. Here, the detected 3-month lag mainly reflects the persistence of the SSTAs rather than the prior occurrence of the SST forcing, as suggested by Frankignoul and Sennéchael (2007). In fact, the eastern centers of action of the SSTA pattern in fall can persist into the early winter, albeit the small magnitudes, in which the southeastern warm center shows a stronger persistence (Fig. 5a). It is also found that such centers, which are expected to change the meridional temperature gradient of atmosphere, have a dominant influence on storm tracks.

When storm tracks lead SST, it is found that a southward shift of storm tracks tends to force significant cold SSTAs in the western and central North Pacific accompanied by warm SSTAs along the western coast of North America during early winter. By analyzing the mixed layer heat budget, the warm SSTAs are found to be primarily determined by the surface heat flux forcing, whereas the cold SSTAs are attributed to both the anomalous heat flux and Ekman cold advection associated with a basin-scale cyclonic wind stress anomaly. Note that the storm-track forcing pattern in early winter is in sharp contrast with the pattern responding to the North Pacific SST in fall, which needs to be understood in further studies.

On interannual and longer time scales, it is found that SST and storm-track anomalies are mutually reinforced during winter, with corresponding anomaly patterns displaying a pronounced decadal variability. The leading EOF of the DJF-mean storm-track anomalies characterizes the decadal variations in the intensity of wintertime storm tracks. This decadal variability of storm tracks is found to be highly associated with the North Pacific decadal mode linearly independent of ENSO, which has been documented in previous studies (Deser and Blackmon 1995; Zhang et al. 1996).

Furthermore, the lagged MCA suggests that the identified coupling between the wintertime storm tracks and SST is active and significant at interannual and longer time scales. When SST leads storm tracks by up to 3 yr, a PDO-like pattern of SSTAs with warming in the western–central North Pacific tend to induce a basin-scale positive storm-track anomaly extending along 50°N with amplitude of $21\,m^2\,s^{-2}\,°C^{-1}$. This is closely related to the lower-tropospheric baroclinicity changes in the high latitudes. In addition, the intensified storm tracks are also found to be physically consistent with the fact that baroclinic eddies effectively tap into more available potential energy. When storm tracks lead SST by up to 4 yr, the basin-scale positive storm-track anomalies to the north of 40°N tend to induce significant warm SSTAs along 40°N, especially in the KOE region, and cold SSTAs in the north of 45°N. These cold SSTAs, particularly in the Gulf

of Alaska, are found to be mainly attributed to the storm-track-induced heat flux forcing. The warm SSTAs in the western–central North Pacific, except in the KOE west of 150°E, are primarily contributed from the anomalous Ekman warm advection. In fact, the decadal variability of SST in the KOE region has been suggested to be induced by the westward propagating planetary waves, which are forced by the anomalous wind stress curl in the central North Pacific (e.g., Seager et al. 2001; Schneider et al. 2002; Kwon and Deser 2007). Note that these MCA patterns for SST and storm tracks bear great similarities at leads and lags, suggesting that a positive feedback between wintertime SST and storm tracks may enhance the decadal climate variability in the North Pacific. Future studies using climate models are clearly needed to understand the mechanisms underlying this coupled relationship.

It is also worth noting that the wintertime storm tracks response to SSTAs in the North Pacific appears to have an opposite sign at seasonal and interannual-to-decadal time scales. This seems reasonable, because at seasonal time scales the winter storm-track anomalies are associated with the preceding fall SSTAs, while at interannual-to-decadal time scales the winter storm-track anomalies are related to the previous winter SSTAs. In fact, when we look at the simultaneous associations between storm tracks and SSTAs in December at seasonal time scales (Fig. 2c), the coupled pattern between SSTAs and storm tracks is consistent with that at interannual-to-decadal time scales (Fig. 9).

The SSTAs in one winter affecting storm tracks in the subsequent winters is likely to be attributed to the large winter-to-winter persistence of SSTAs, especially in the KOE region. Previous studies have documented that this persistence can be interpreted by the ''re-emergence mechanism'' involving the seasonality of the mixed layer depth (e.g., Alexander and Deser 1995; Alexander et al. 1999; Hanawa and Sugimoto 2004). In addition, the SSTAs in the subarctic frontal zone are found to play an important role in the development of storm tracks and thus in the midlatitude air–sea interactions (e.g., Nakamura et al. 2004; Sampe et al. 2010; Taguchi et al. 2012). As seen in Fig. 12, the SSTAs in the KOE region indeed show a strong winter-to-winter persistence.

Acknowledgments. This work is supported by China National Global Change Major Research Project (2013CB956201), National Natural Science Key Research Project (41130859), and Innovation and Research Foundation of Ocean University of China (201261011). We appreciate two anonymous reviewers for their suggestions to improve the manuscript substantially.

REFERENCES

Alexander, M. A., and C. Deser, 1995: A mechanism for the recurrence of wintertime midlatitude SST anomalies. *J. Phys. Oceanogr.,* **25,** 122–137.

——, ——, and M. S. Timlin, 1999: The reemergence of SST anomalies in the North Pacific Ocean. *J. Climate,* **12,** 2419–2433.

——, I. Blade, M. Newman, J. R. Lanzante, N.-C. Lau, and J. D. Scott, 2002: The atmospheric bridge: The influence of ENSO teleconnections on air–sea interaction over the global oceans. *J. Climate,* **15,** 2205–2231.

Blackmon, M. L., J. M. Wallace, N. C. Lau, and S. L. Mullen, 1977: An observational study of the Northern Hemisphere wintertime circulation. *J. Atmos. Sci.,* **34,** 1040–1053.

Cai, M., S. Yang, H. M. Van den Dool, and V. E. Kousky, 2007: Dynamical implications of the orientation of atmospheric eddies: A local energetics perspective. *Tellus,* **59A,** 127–140.

Carton, J. A., and B. S. Giese, 2008: A reanalysis of ocean climate using Simple Ocean Data Assimilation (SODA). *Mon. Wea. Rev.,* **136,** 2999–3017.

Chang, E. K. M., 2001: GCM and observational diagnoses of the seasonal and interannual variations of the Pacific storm track during the cool season. *J. Atmos. Sci.,* **58,** 1784–1800.

——, and Y. Fu, 2002: Interdecadal variations in Northern Hemisphere winter storm track intensity. *J. Climate,* **15,** 642–658.

——, S. Lee, and K. L. Swanson, 2002: Storm track dynamics. *J. Climate,* **15,** 2163–2183.

Christoph, M., U. Ulbrich, and P. Speth, 1997: Midwinter suppression of Northern Hemisphere storm track activity in the real atmosphere and in GCM experiments. *J. Atmos. Sci.,* **54,** 1589–1599.

Compo, G. P., and Coauthors, 2011: The Twentieth Century Reanalysis Project. *Quart. J. Roy. Meteor. Soc.,* **137,** 1–28, doi:10.1002/qj.776.

Czaja, A., and C. Frankignoul, 2002: Observed impact of Atlantic SST anomalies on the North Atlantic Oscillation. *J. Climate,* **15,** 606–623.

Deser, C., and M. L. Blackmon, 1995: On the relationship between tropical and North Pacific sea surface temperature variations. *J. Climate,* **8,** 1677–1680.

Donat, M. G., D. Renggli, S. Wild, L. V. Alexander, G. C. Leckebusch, and U. Ulbrich, 2011: Reanalysis suggests long-term upward trends in European storminess since 1871. *Geophys. Res. Lett.,* **38,** L14703, doi:10.1029/2011GL047995.

Frankignoul, C., and N. Sennéchael, 2007: Observed influence of North Pacific SST anomalies on the atmospheric circulation. *J. Climate,* **20,** 592–606.

——, ——, Y. Kwon, and M. A. Alexander, 2011: Influence of the meridional shifts of the Kuroshio and the Oyashio Extensions on the atmospheric circulation. *J. Climate,* **24,** 762–777.

Gastineau, G., and C. Frankignoul, 2012: Cold-season atmospheric response to the natural variability of the Atlantic meridional overturning circulation. *Climate Dyn.,* **39,** 37–57.

Hanawa, K., and S. Sugimoto, 2004: 'Reemergence' areas of winter sea surface temperature anomalies in the world's oceans. *Geophys. Res. Lett.,* **31,** L10303, doi:10.1029/2004GL019904.

Kelly, K. A., and S. Dong, 2004: The relationship of western boundary current heat transport and storage to mid-latitude ocean–atmosphere interaction. *Earth's Climate: The Ocean–Atmosphere Interaction, Geophys. Monogr.,* Vol. 147, Amer. Geophys. Union, 347–363.

Kug, J. S., F. F. Jin, J. H. Par, H. L. Ren, and I. S. Kang, 2010: A general rule for synoptic-eddy feedback onto low-frequency flow. *Climate Dyn.,* **35,** 1011–1026.

Kushnir, Y., W. A. Robinson, I. Blade, N. M. J. Hall, S. Peng, and R. Sutton, 2002: Atmospheric GCM response to extratropical SST anomalies: Synthesis and evaluation. *J. Climate,* **15,** 2233–2256.

Kwon, Y.-O., and C. Deser, 2007: North Pacific decadal variability in the Community Climate System Model version 2. *J. Climate,* **20,** 2416–2433.

Latif, M., and T. P. Barnett, 1994: Causes of decadal climate variability over the North Pacific and North America. *Science,* **266,** 634–637.

Lau, N. C., and E. O. Holopainen, 1984: Transient eddy forcing of the time-mean flow as identified by geopotential tendencies. *J. Atmos. Sci.,* **41,** 313–328.

Lee, S. S., J. Y. Lee, B. Wang, K. J. Ha, K. Y. Heo, F. F. Jin, D. M. Straus, and J. Shukla, 2011: Interdecadal changes in the storm track activity over the North Pacific and North Atlantic. *Climate Dyn.,* **39,** 313–327.

Lindzen, R. S., and B. F. Farrell, 1980: A simple approximation result for maximum growth rate of baroclinic instabilities. *J. Atmos. Sci.,* **37,** 1648–1654.

Mantua, N. J., S. R. Hare, Y. Zhang, J. M. Wallace, and R. C. Francis, 1997: A Pacific interdecadal climate oscillation with impacts on salmon production. *Bull. Amer. Meteor. Soc.,* **78,** 1069–1079.

Mizuta, R., M. Matsueda, H. Endo, and S. Yukimoto, 2011: Future change in extratropical cyclones associated with change in the upper troposphere. *J. Climate,* **24,** 6456–6470.

Nakamura, H., 1992: Midwinter suppression of baroclinic wave activity in the Pacific. *J. Atmos. Sci.,* **49,** 1629–1642.

——, T. Izumi, and T. Sampe, 2002: Interannual and decadal modulations recently observed in the Pacific storm track activity and East Asian winter monsoon. *J. Climate,* **15,** 1855–1874.

——, T. Sampe, Y. Tanimoto, and A. Shimpo, 2004: Observed associations among storm tracks, jet streams and midlatitude oceanic fronts. *Earth's Climate: The Ocean–Atmosphere Interaction, Geophys. Monogr.,* Vol. 147, Amer. Geophys. Union, 329–346.

Nakamura, M., and S. Yamane, 2010: Dominant anomaly patterns in the near-surface baroclinicity and accompanying anomalies in the atmosphere and oceans. Part II: North Pacific basin. *J. Climate,* **23,** 6445–6467.

Peng, S., and J. S. Whitaker, 1999: Mechanisms determining the atmospheric response to midlatitude SST anomalies. *J. Climate,* **12,** 1393–1408.

Pinto, J. G., M. Reyers, and U. Ulbrich, 2011: The variable link between PNA and NAO in observations and in multi-century CGCM simulations. *Climate Dyn.,* **36,** 337–354.

Qiu, B., 2000: Interannual variability of the Kuroshio Extension system and its impact on the wintertime SST field. *J. Phys. Oceanogr.,* **30,** 1486–1502.

Rayner, N. A., D. E. Parker, E. B. Horton, C. K. Folland, L. V. Alexander, D. P. Rowell, E. C. Kent, and A. Kaplan, 2003: Global analyses of sea surface temperature, sea ice, and night marine air temperature since the late nineteenth century. *J. Geophys. Res.,* **108,** 4407, doi:10.1029/2002JD002670.

Rivière, G., and I. Orlanski, 2007: Characteristics of the Atlantic storm-track eddy activity and its relation with the North Atlantic Oscillation. *J. Atmos. Sci.,* **64,** 241–266.

Sampe, T., H. Nakamura, A. Goto, and W. Ohfuchi, 2010: Significance of a midlatitude SST frontal zone in the formation of a storm track and an eddy-driven westerly jet. *J. Climate,* **23,** 1793–1814.

Schneider, N., A. J. Miller, and D. W. Pierce, 2002: Anatomy of North Pacific decadal variability. *J. Climate,* **15,** 586–605.

Seager, R., Y. Kushnir, N. Naik, M. A. Cane, and J. A. Miller, 2001: Wind-driven shifts in the latitude of the Kuroshio–Oyashio Extension and generation of SST anomalies on decadal time scales. *J. Climate,* **14,** 4249–4265.

Taguchi, B., H. Nakamura, M. Nonaka, and S.-P. Xie, 2009: Influences of the Kuroshio/Oyashio Extensions on air–sea heat exchanges and storm-track activity as revealed in regional atmospheric model simulations for the 2003/04 cold season. *J. Climate,* **22,** 6536–6560.

——, ——, ——, N. Komori, A. Kuwano-Yoshida, K. Takaya, and A. Goto, 2012: Seasonal evolutions of atmospheric response to decadal SST anomalies in the North Pacific subarctic frontal zone: Observations and a coupled model simulation. *J. Climate,* **25,** 111–139.

Trenberth, K. E., and J. W. Hurrell, 1994: Decadal atmosphere-ocean variations in the Pacific. *Climate Dyn.,* **9,** 303–319.

Wu, L., Z. Liu, R. Gallimore, R. Jacob, D. Lee, and Y. Zhong, 2003: A coupled modeling study of Pacific decadal variability: The tropical mode and the North Pacific mode. *J. Climate,* **16,** 1101–1120.

Wu, Y., M. Ting, R. Seager, H. P. Huang, and M. A. Cane, 2011: Changes in storm tracks and energy transports in a warmer climate simulated by the GFDL CM2.1 model. *Climate Dyn.,* **37,** 53–72.

Yin, J. H., 2005: A consistent poleward shift of the storm tracks in simulations of 21st century climate. *Geophys. Res. Lett.,* **32,** L18701, doi:10.1029/2005GL023684.

Zhang, Y., and I. M. Held, 1999: A linear stochastic model of a GCM's midlatitude storm tracks. *J. Atmos. Sci.,* **56,** 3416–3435.

——, J. M. Wallace, and N. Iwasaka, 1996: Is climate variability over the North Pacific a linear response to ENSO? *J. Climate,* **9,** 1468–1478.